Available online at www.sciencedirect.com
ScienceDirect
Journal of Solid State Chemistry 180 (2007) 1149–1157
JOURNAL OF SOLID STATE CHEMISTRY
www.elsevier.com/locate/jssc

Hydrothermal synthesis and crystal structure of the $Ni_2(C_4H_4N_2)(V_4O_{12})(H_2O)_2$ and $Ni_3(C_4H_4N_2)_3(V_8O_{23})$ inorganic–organic hybrid compounds. Thermal, spectroscopic and magnetic studies of the hydrated phase

Edurne S. Larrea[a], José L. Mesa[a,*], José L. Pizarro[b], María I. Arriortua[b], Teófilo Rojo[a]

[a]*Dpto. de Química Inorgánica, Facultad de Ciencia y Tecnología, Universidad del País Vasco, Apdo. 644, E-48080 Bilbao, Spain*
[b]*Dpto. de Mineralogía y Petrología, Facultad de Ciencia y Tecnología, Universidad del País Vasco, Apdo. 644, E-48080 Bilbao, Spain*

Received 3 November 2006; received in revised form 20 December 2006; accepted 30 December 2006
Available online 24 January 2007

Abstract

$Ni_2(C_4H_4N_2)(V_4O_{12})(H_2O)_2$, **1**, and $Ni_3(C_4H_4N_2)_3(V_8O_{23})$, **2**, have been synthesized using mild hydrothermal conditions at 170 °C under autogenous pressure. Both phases crystallize in the *P*-1 triclinic space group, with the unit-cell parameters, $a = 7.437(7)$, $b = 7.571(3)$, $c = 7.564(4)$ Å, $\alpha = 65.64(4)$, $\beta = 76.09(4)$, $\gamma = 86.25(3)^\circ$ for **1** and $a = 8.566(2)$, $b = 9.117(2)$, $c = 12.619(3)$ Å, $\alpha = 71.05(2)$, $\beta = 83.48(4)$, $\gamma = 61.32(3)^\circ$ for **2**, being $Z = 2$ for both compounds. The crystal structure of the three-dimensional **1** is constructed from layers linked between them through the pyrazine molecules. The sheets are formed by edge-shared $[Ni_2O_6(H_2O)_2N_2]$ nickel(II) dimers octahedra and rings composed by four $[V_4O_{12}]$ vanadium(V) tetrahedra linked through vertices. The crystal structure of **2** is formed from vertex shared $[VO_4]$ tetrahedra that give rise to twelve member rings. $[NiO_4(C_4H_4N_2)_2]_\infty$ chains, resulting from $[NiO_4N_2]$ octahedra and pyrazine molecules, give rise to a 3D skeleton when connecting to $[VO_4]$ tetrahedra. Diffuse reflectance measurements of **1** indicate a slightly distorted octahedral geometry with values of $Dq = 880$, $B = 980$ and $C = 2700\,cm^{-1}$. Magnetic measurements of **1**, carried out in the 5.0–300 K range, indicate the existence of antiferromagnetic couplings with a Neel temperature near to 38 K.

Keywords: Hydrothermal synthesis; Inorganic-organic hybrid compounds; Thermal Study; IR; Diffuse reflectance; Magnetism

1. Introduction

Although the vanadium oxides have been well documented to exhibit interesting intercalation, electronic and magnetic properties, it is only recently that attention has been drawn to the synthesis and structure of such new compounds that are templated by organic amines [1]. Examples of vanadium oxides templated or coordinated by transition metal complexes, however, are still rare. They include one-dimensional metavanadate chain compounds $Cu(NH_3)_2V_2O_6$, $Cu(en)V_2O_6$, $Cu(bipy)V_2O_6$ [2] and $Cu(bipy)_2V_2O_6$ [3], where the co-ordination groups are attached to the V–O chains. Layered mixed-valence vanadium oxides have also been found in $[Cu(en)_2][V_6O_{14}]$, $[Cu(en)_2]_2[V_{10}O_{25}]$, $[Zn(bipy)_2]_2[V_6O_{17}]$ and $[Zn(en)_2][V_6O_{14}]$ [4], where the copper(II) or zinc(II) complexes reside between V–O layers as charge compensating templates. Owing to the ability of vanadium to adopt a variety of co-ordination geometries in various oxidation states, the influences of the second metal ions as well as the organic ligands on the structures could be significant. Therefore, novel structural types could be discovered by modifying the transition metal ions, the organic groups and the synthetic conditions.

On the other hand, the vanadium oxides which contain transition metal complexes may be of interest in magnetism. A variety of magnetic systems with different kinds of

*Corresponding author. Fax: +34 946013500.
E-mail address: joseluis.mesa@ehu.es (J.L. Mesa).

0022-4596/$ - see front matter © 2007 Elsevier Inc. All rights reserved.
doi:10.1016/j.jssc.2006.12.037

interacting ions and increased nuclearities could be obtained. These systems can be sometimes well isolated by the diamagnetic vanadium oxides, and thus allow for a detailed investigation of their magneto–structural relationships.

In this work we report on the hydrothermal synthesis and crystal structures of the three-dimensional $Ni_2(C_4H_4N_2)(V_4O_{12})(H_2O)_2$ **1** and $Ni_3(C_4H_4N_2)_3(V_8O_{23})$ **2** phases. A thermal, spectroscopic and magnetic study of compound **1** is also carried out.

2. Experimental

2.1. Synthesis and characterization

$Ni_2(C_4H_4N_2)(V_4O_{12})(H_2O)_2$ **1** and $Ni_3(C_4H_4N_2)_3(V_8O_{23})$ **2** have been synthesized using mild hydrothermal conditions at 170 °C and a pressure between 10 and 20 bars, employing PTFE (poly-tetrafluoroethylene) reactors. The starting reagents were $Ni(NO_3)_2 \cdot 6H_2O$, $NaVO_3$, $C_4H_4N_2$ (pyrazine) solved in water, and 1 M HCl solution in a molar ratio of 1:1:1:1:49121, giving a pH of 3.0. After five days of reaction, a mixture of green prismatic single-crystals of both compounds **1** and **2** was obtained. The variation of pH up to a value of 6.0 and the stoichiometric amounts of $Ni(NO_3)_2 \cdot 6H_2O$ (0.50 mmol), $NaVO_3$ (0.50 mmol), $C_4H_4N_2$ (0.50 mmol) allowed to obtain **1** as a pure phase, yield, approximately, 85%. Attempts to carry out the attainment of compound **2** as pure phase with different pH and several amounts of the mentioned reagents were unsuccessful.

The amounts of nickel and vanadium in compound **1** were measured by atomic absorption spectrophotometry. C, N and H elemental analysis was used to calculate the amounts of these elements. $Ni_2(C_4H_4N_2)(V_4O_{12})(H_2O)_2$ requires: Ni 18.6; V, 32.4; C, 7.6; N, 4.4; H, 1.3. Found Ni, 18.2; V, 31.8; C, 7.5; N, 4.2; H, 1.1. The small amount obtained of phase **2** precluded to carry out the chemical analysis of this phase. The formula was deduced from the analysis of the single crystal X-ray diffraction data. The densities of both compounds were measured by the flotation method, using a mixture of CH_2I_2 and CH_2Cl_2, being the densities 2.70 for **1** and 2.41 g cm^{-3} for **2**.

The IR spectrum of compound **1** was performed in the 4000–400 cm^{-1} range. At 3360 cm^{-1} the stretching vibration of the OH groups of the water molecule is observed. The deformation mode of this molecule appears at 1460 cm^{-1}. The bands due to the $(VO_4)^{3-}$ vanadate group appear in the 939–400 cm^{-1} range. The signal observed at 925 cm^{-1} was attributed to the stretching vibration of V–O terminal bonds. At 895 and 865 cm^{-1} two bands of medium intensity corresponding to the antisymmetric stretching vibration of the V–O–V bonds can be distinguished. The symmetric stretching vibration of this group appears at 555 and 475 cm^{-1}. The stronger band of the spectrum corresponds to the antisymmetric stretching vibration of the $(VO_4)^{3-}$ anion at 770 cm^{-1}[5]. The bands due to the pyrazine ligand appear in the 1650–970 cm^{-1} range, together with a set of very weak bands at 3215 and 3110 cm^{-1} assigned to the stretching vibration of the C–H bonds from the aromatic ring. The bands with medium intensity at 1630 and 1050 cm^{-1} are due to the stretching vibrations in the plane of the ring from the C = C and C = N bonds. Finally, the band observed at 970 cm^{-1} is attributed to the stretching vibration of the aromatic ring.

The thermogravimetric analysis (TGA) was performed under synthetic air in a DSC simultaneous differential scanning calorimetry (DSC)-TGA TA instrument. A crucible containing approximately 20 mg of sample was heated at 5 °C min^{-1} in the temperature range 30–800 °C. The decomposition curve of **1** shows two processes of mass loss. The first one, with endothermic character, is observed between 280 and 370 °C and corresponds to a mass loss of 5.6%. This loss is attributed to the elimination of the water molecule from the structure, the theoretical loss is 5.7%. The second process occurs between 415 and 445 °C and supposes a mass loss of 12.3% in good agreement with the calcination of the pyrazine molecule (12.7% in mass) to give CO(g) which is transformed to CO_2(g), in air. The global decomposition of the pyrazine molecule shows exothermic character. The inorganic residue at 500 °C was identified by X-ray powder diffraction analysis. This residue corresponds to the $Ni(V_2O_6)$, ICDD 76-0359 [6a].

The thermal behavior of **1** was also studied by using time-resolved X-ray thermodiffractometry in synthetic air. A Philips X'PERT automatic diffractometer (Cu$K\alpha$ radiation) equipped with a variable-temperature stage (Paar Physica TCU2000) with a Pt sample holder was used in the experiment. The powder patterns were recorded in 2θ steps of 0.06° in the $5 \leqslant 2\theta \leqslant 35$, counting for 2 s per step and increasing the temperature at 5 °C min^{-1} from room temperature to 805 °C. In the thermodiffractogram, shown in Fig. 1, four different steps can be observed. Phase **1** maintains its stability up to 280 °C. Above this temperature the peaks of this phase lose intensity and other different peaks belonging to an intermediate unknown phase appear. This unknown phase results as a product from the elimination of the water molecules, coexisting with the $Ni(V_2O_6)$ compound at 415 °C, ICDD 76-0359 [6a], but it rapidly disappears at approximately 450 °C. Finally, at 745 °C the $Ni_2(V_2O_7)$, ICDD 38-0285 [6b] is observed.

2.2. Single-crystal X-ray diffraction study

Prismatic single crystals of compounds **1** and **2** with dimensions $0.26 \times 0.10 \times 0.04$ and $0.12 \times 0.06 \times 0.04$ mm, respectively, were carefully selected under a polarizing microscope and mounted on a glass fiber. Diffraction data were collected on an Oxford Diffraction Xcalibur2 using graphite monochromated Mo$K\alpha$ radiation. Details of crystal data, intensity collection, and some features of the structural refinement are reported in Table 1.

Correction for Lorentz and polarization effects were done and also for absorption with the empirical Ψ scan

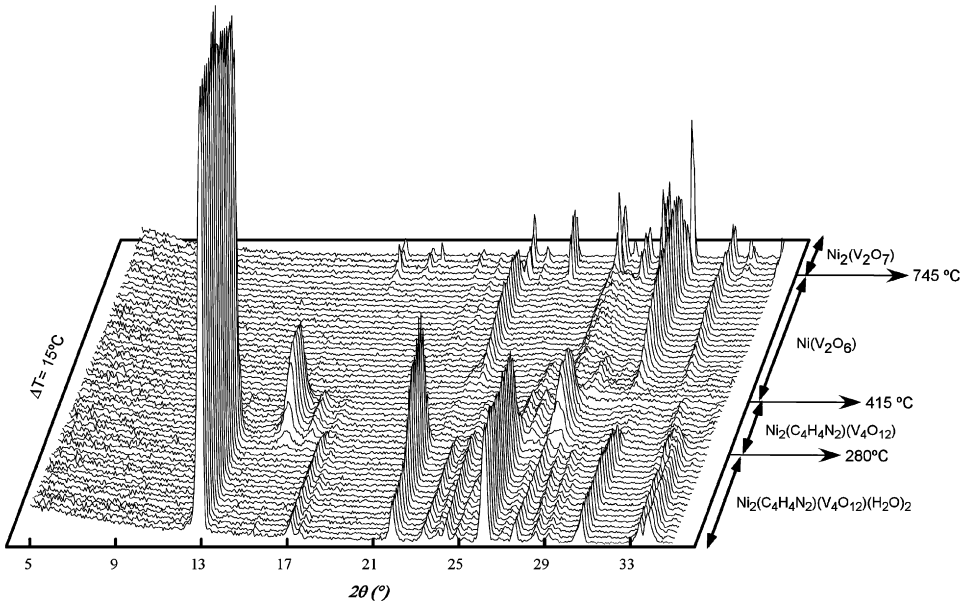

Fig. 1. Thermodiffractograms of the compound **1**.

Table 1
Details of the crystal data, structural resolution and refinement procedure for **1** and **2**

Formula	$C_2\ H_4\ N\ Ni\ O_7\ V_2$	$C_6\ H_6\ N_3\ Ni_{1.5}\ O_{11.5}V_4$
Molecular weight ($g\,mol^{-1}$)	314.65	595.96
Crystalline system	Triclinic	Triclinic
Space group (No.)	P-1 (2)	P-1 (2)
a (Å)	7.437(3)	8.556(2)
b (Å)	7.571(3)	9.117(2)
c (Å)	7.756(4)	12.619(3)
α (°)	65.64(4)	71.05(2)
β (°)	76.09(4)	83.48(2)
γ (°)	86.25(3)	61.32(3)
V ($Å^3$)	385.9(3)	815.7(3)
Z	2	2
ρ_{obs}, ρ_{calc} ($gr\,cm^{-3}$)	2.70(1), 2.708	2.41(1), 2.426
$F(000)$	306	578
Collection data		
Temperature, K	293(2)	293(2)
Diffractometer	Oxford Diffraction Xcalibur2	
μ (mm^{-1})	4.790	3.962
Radiation, λ(Mo$K\alpha$) (Å)	0.71073	0.71073
Crystal size (mm)	$0.26 \times 0.10 \times 0.04$	$0.12 \times 0.06 \times 0.04$
Range θ (°)	4.17-26.01	2.87-26.37
Interval h, k, l	$-7 \leqslant h \leqslant 9$, $-9 \leqslant k \leqslant 9$, $-9 \leqslant l \leqslant 9$	$-10 \leqslant h \leqslant 8$, $-11 \leqslant k \leqslant 10$, $-15 \leqslant l \leqslant 15$
No of measured reflections	2775	6134
No of independent reflections	1491	3269
R (int)	0.0901	0.0376
Refinement		
Data/Restrictions/Parameter	1491/2/125	3269/0/238
R factors [$I > 2\sigma(I)$]	$R1 = 0.0506$ $wR_2 = 0.1249$	$R1 = 0.0272$ $wR_2 = 0.0409$
R factors [all data]	$R1 = 0.0535$ $wR_2 = 0.1277$	$R1 = 0.0460$ $wR_2 = 0.0439$
Max. and min. of electronic residual density ($e.Å^{-3}$)	0.876, −0.878	0.411, −0.359
G. O. F	1.015	0.901

$$R1 = \frac{\sum ||F_o| - |F_c||}{\sum |F_o|};\ wR2 = \sqrt{\frac{\sum w(|F_o| - |F_c|)^2}{\sum w|F_o|^2}}$$

$w = 1/[\sigma^2|Fo|^2 + (xp)^2 + yp]$ with $p = [\max|Fo|^2 + 2|Fc|^2]/3$, where $x = 0.0912$, $y = 0$; for **1**. and $x = 0.0045$, $y = 0$ for **2**.

Table 2
Selected bond distances (Å) and angles (°) for **1**

Bond distances					
$Ni(1)O_5N$ octahedron		$V(1)O_4$ tetrahedron		$V(2)O_4$ tetrahedron	
Ni1–O(7w)	2.055(3)	V1–O(3)	1.619(3)	V2–O(5)^{ii}	1.664(3)*
Ni1–O(1)^{I}	2.063(3)*	V1–O(1)	1.709(3)*	V2–O(6)^{i}	1.678(3)*
Ni1–N(1)	2.082(4)	V1–O(4)	1.789(3)*	V2–O(2)^{iii}	1.789(3)*
Ni1–O(6)	2.095(3)*	V1–O(2)	1.825(3)*	V2–O(4)^{iv}	1.806(3)*
Ni1–O(1)	2.102(3)*				
Ni1–O(5)^{ii}	2.107(3)*				
($C_4H_4N_2$) pyrazine					
N(1)–C(2) 1.353(6)		N(1)–C(1) 1.361(6)		C(1)–C(2)^{vi} 1.383(7)	
C(1)–H(1) 0.930		C(2)–C(1)^{vi} 1.383(7)		C(2)–H(2) 0.930	
Bond angles					
$N(1)O_4N$ octahedron		$V(1)O_4$ tetrahedron		$V(2)O_4$ tetrahedron	
O(7w)–Ni1–O(1)^{i}	94.3(1)	O(3)–V1–O(1)	109.2(2)	O(5)^{ii}-V2–O(6)^{i}	110.9(2)*
O(7w)–Ni1–N(1)	88.2(1)	O(3)–V1–O(4)	108.7(2)	O(5)^{ii}-V2–O(2)^{iii}	109.0(2)*
O(1)^{i}-Ni1–N(1)	177.3(1)	O(1)–V1–O(4)	111.9(1)*	O(6)^{i}-V2–O(2)^{iii}	110.8(2)*
O(7w)–Ni1–O(6)	94.0(1)	O(3)–V1–O(2)	109.7(2)	O(5)^{ii}-V2–O(4)^{iv}	110.1(1)*
O(1)^{i}-Ni1–O(6)	85.8(1)	O(1)–V1–O(2)	107.7(1)*	O(6)^{i}-V2–O(4)^{iv}	109.6(2)*
N(1)–Ni1–O(6)	94.9(6)	O(4)–V1–O(2)	109.5(2)	O(2)^{iii}-V2–O(4)^{iv}	106.1(2)*
O(7w)–Ni1–O(1)	174.7(1)				
O(1)^{i}-Ni1–O(1)	84.0(1)	($C_4H_4N_2$) pyrazine			
N(1)–Ni1–O(1)	93.3(1)	C(2)–N1-C(1)	117.6(4)		
O(6)–Ni1–O(1)	90.9(1)	C(2)–N1-Ni(1)	118.9(3)		
O(7w)–Ni1–O(5)^{ii}	91.0(1)	C(1)–N1-Ni(1)	123.4(3)		
O(1)^{i}-Ni1–O(5)^{ii}	85.4(1)	N(1)–C1-C(2)^{vi}	121.2(4)		
N(1)–Ni1–O(5)^{ii}	93.6(1)	C(2)^{vi}-C1-H(1)	119.4(1)		
O(6)–Ni1–O(5)^{ii}	170.2(1)	N(1)–C2-C(1)^{vi}	121.1(4)		
O(1)–Ni1–O(5)^{ii}	83.9(1)	N(1)–C2-H(2)	119.4(1)		
		C(1)^{vi}–C2-H(2)	119.4(1)		
Other bond angles involved in the exchange magnetic pathways					
Ni–O(5)–V(2)	127.7(2)			Ni–O(6)–V(2)	123.4(3)
V(2)–O(4)–V(1)	128.7(3)			V(1)–O(1)–Ni	127.8(3)
V(1)–O(1)–Ni	132.8(3)			Ni–O(1)–Ni	95.95(1)
V(1)–O(2)–V(2)	151.5(2)				

Symmetry codes: i = $-x+1,-y,-z$; ii = $x,y,z-1$; iii = $x,y-1,z$; iv = $-x,-y,-z$; v = $x,y+1,z$; vi = $-x,-y,-z+1$.The asterisk indicates the bond distances and angles involved in the exchange magnetic pathways.

method [7] by using the CRYSALIS program [8]. Direct methods (SHELXS 97) [9] were employed to solve the structures and then refined by the full-matrix least-squares procedure based on F^2, using the SHELXL 97 computer program [10] belonging to the WINGX software package [11]. The scattering factors were taken from Ref. [12]. Anisotropic thermal parameters were assigned to the non-H atoms. In Table 1 the final *R* factors are given for **1** and **2** compounds, respectively. A simulation based on the single-crystal structure was in excellent agreement with the X-ray powder data, indicating the presence of a pure phase with high crystallinity in the case of compound **1**. Selected bond distances and angles are shown in Tables 2 and 3.

2.3. Physicochemical characterization techniques

The IR spectrum (KBr pellets) was obtained with a Nicolet FT-IR 740 spectrophotometer. The diffuse reflectance spectrum was registered at room temperature on a Cary 5000 spectrometer in the 200–2000 nm range. Magnetic measurements on powdered sample were performed in the temperature range 5.0–300 K, using a Quantum Design MPMS-7 SQUID magnetometer. The magnetic field was 1000 Oe, a value in the range of linear dependence of magnetization vs. magnetic field, even at 5.0 K.

3. Results and discussion

3.1. Crystal structure of phase 1

The three-dimensional crystal structure of the $Ni_2(C_4H_4N_2)(V_4O_{12})(H_2O)_2$ compound is built from layers linked between them through the pyrazine molecules. The sheets are formed by $[Ni_2O_6(H_2O)_2N_2]$ edge-shared nickel(II) dimer octahedra and rings which contain four $[V_4O_{12}]$ vanadium(V) tetrahedra linked through vertices. The dimeric octahedra and the ring of tetrahedra are linked

Table 3
Selected bond distances (Å) and angles (°) for 2

Bond distances					
$Ni(1)O_4N_2$ octahedron		$Ni(2)O_4N_2$ octahedron		$V(1)O_4$ tetrahedron	
N1–O(7)^{i} 2.028(2)		Ni2–O(11) 2.034(2)		V1–O(2)^{iv}1.648(2)	
Ni1–O(7)^{ii} 2.028(2)		Ni2–O(4) 2.058(2)		V1–O(4) 1.659(2)	
Ni1–O(6)^{i} 2.054(2)		Ni2–O(2) 2.069(2)		V1–O(3) 1.800(2)	
Ni1–O(6)^{ii} 2.0542(2)		Ni2–N(1) 2.080(2)		V1–O(1) 1.831(2)	
Ni1–N(2) 2.0952(2)		Ni2–O(10) 2.091(2)			
Ni1–N(2)^{iii}2.095(2)		Ni2–N(3) 2.106(2)			
$V(2)O_4$ tetrahedron		$V(3)O_4$ tetrahedron		$V(4)O_4$ tetrahedron	
V2–O(10) 1.649(2)		V3–O(7) 1.643(2)		V4–O(9) 1.599(2)	
V2–O(6) 1.663(2)		V3–O(11) 1.658(2)		V4–O(5) 1.770(2)	
V2–O(3)^{iv} 1.790(2)		V3–O(12) 1.7833(9)		V4–O(1)^{v} 1.773(2)	
V2–O(5)1.819(2)		V3–O(8) 1.821(2)		V4–O(8)^{vi}1.781(2)	
$(C_4H_4N_2)$ pyrazine					
N(1)–C(1)	1.337(4)	N(1)–C(4)	1.351(4)	N(2)–C(3)	1.338(4)
N(2)–C(2)	1.349(4)	N(3)–C(5)	1.332(4)	N(3)–C(6)^{x}	1.347(4)
C(1)–C(2)	1.393(4)	C(5)–C(6)	1.387(4)	C(6)–N(3)^{x}	1.347(4)
Bond angles					
$Ni(1)O_4N_2$ octahedron		$Ni(2)O_4N_2$ octahedron			
O(7)^{i}–Ni1–O(7)^{ii}	180.0(0)	O(11)–Ni2–O(4)		178.49(8)	
O(7)^{i}–Ni1–O(6)^{i}	90.14(9)	O(11)–Ni2–O(4)		90.29(8)	
O(7)^{ii}–Ni1–O(6)^{i}	89.86(9)	O(4)–Ni2–O(2)		89.50(8)	
O(7)^{i}–Ni1–O(6)^{ii}	89.86(9)	O(11)–Ni2-N(1)		91.91(9)	
O(7)^{ii}–Ni1–O(6)^{ii}	90.14(9)	O(4)–Ni2-N(1)		88.43(9)	
O(6)^{i}–Ni1–O(6)^{ii}	180.0(0)	O(2)–Ni2-N(1)		174.95(9)	
O(7)^{i}-Ni1–N(2)	99.14(9)	O(11)–Ni2–O(10)		89.26(8)	
O(7)^{ii}-Ni1–N(2)	90.86(9)	O(4)–Ni2–O(10)		92.23(8)	
O(6)^{i}-Ni1–N(2)	88.71(9)	O(2)–Ni2–O(10)		89.48(8)	
O(6)^{ii}-Ni1–N(2)	91.29(9)	N(1)–Ni2–O(10)		86.00(9)	
O(7)^{i}–Ni1–N(2)^{iii}	90.86(9)	O(11)–Ni2–N(3)		89.34(9)	
O(7)^{ii}–Ni1–N(2)^{iii}	89.14(9)	O(4)–Ni2–N(3)		89.16(9)	
O(6)^{i}–Ni1–N(2)^{iii}	91.29(9)	O(2)–Ni2–N(3)		86.02(9)	
O(6)^{ii}–Ni1–N(2)^{iii}	88.71(9)	N(1)–Ni2–N(3)		98.55(9)	
N(2)–Ni1–N(2)^{iii}	180.0(0)	O(10)–Ni2–N(3)		175.28(9)	
$V(1)O_4$ tetrahedron	$V(2)O_4$ tetrahedron				
O(2)^{iv}-V1–O(4)	111.5(1)	O(10)–V2–O(6)		111.3(1)	
O(2)^{iv}-V1–O(3)	107.6(1)	O(10)–V2–O(3)^{iv}		107.8(1)	
O(4)–V1–O(3)	106.1(1)	O(6)–V2–O(3)^{iv}		107.2(1)	
O(2)^{iv}-V1–O(1)	108.8(1)	O(10)–V2–O(5)		109.9(1)	
O(4)–V1–O(1)	114.1(1)	O(6)–V2–O(5)		108.4(1)	
O(3)–V1–O(1)	108.41(9)	O(3)^{iv}–V2–O(5)		112.39(9)	
$V(3)O_4$ tetrahedron		$V(4)O_4$ tetrahedron			
O(7)–V3–O(11)	109.3(1)	O(9)–V4–O(5)		110.2(1)	
O(7)–V3–O(12)	110.05(8)	O(9)–V4–O(1)^{v}		109.4(1)	
O(11)–V3–O(12)	109.71(8)	O(5)–V4–O(1)^{v}		108.5(1)	
O(7)–V3–O(8)	105.4(1)	O(9)–V4–O(8)^{vi}		107.7(2)	
O(11)–V3–O(8)	108.2(1)	O(5)–V4–O(8)^{vi}		109.1(1)	
O(12)–V3–O(8)	113.96(8)	O(1)^{v}–V4–O(8)^{vi}		112.0(1)	
$(C_4H_4N_2)$ pyrazine					
C(1)–N1-C(4)	117.1(3)				
C(1)–N1–Ni(2)	118.4(2)				
C(4)–N1–Ni(2)	124.4(2)				
C(3)–N2–C(2)	116.9(3)				
C(3)–N2–Ni(1)	122.7(2)				
C(2)–N2–Ni(1)	120.5(2)				
C(5)–N3–C(6)^{x}	116.1(2)				
C(5)–N3–Ni(2)	119.7(2)				
C(6)^{x}–N3–Ni(2)	123.6(2)				
N(1)–C1–C(2)	121.8(3)				
N(2)–C2–C(1)	120.9(3)				
N(2)–C3–C(4)	122.4(3)				
N(1)–C4–C(3)	120.9(3)				
N(3)–C5–C(6)	123.0(3)				
N(3)^{x}–C6–C(5)	120.9(3)				

Symmetry codes: i = $-x+2,-y+1,-z$; ii = $x,y+1,z$; iii = $-x+2,-y+2,-z$; iv = $-x+2,-y,-z+1$; v = $-x+3,-y,-z+1$; vi = $x+1,y,z$; vii = $x,y-1,-z+1$; viii = $x-1,-y+1,-z$; ix = $-x+1,-y+1,-z$; x = $-x+1,-y+1,-z+1$.

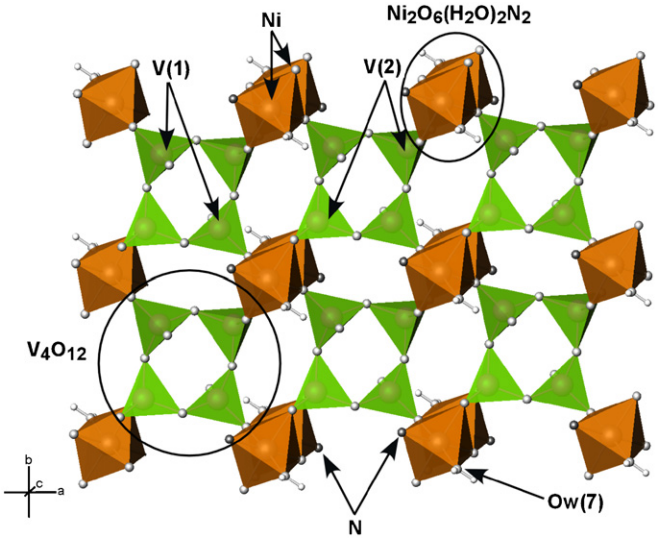

Fig. 2. Polyhedral view in the *ab*-plane of the crystal structure of **1** showing the layers constructed from nickel(II) dimmers and the rings formed by $[V_4O_{12}]$ vanadium(V) tetrahedra, inside the circles.

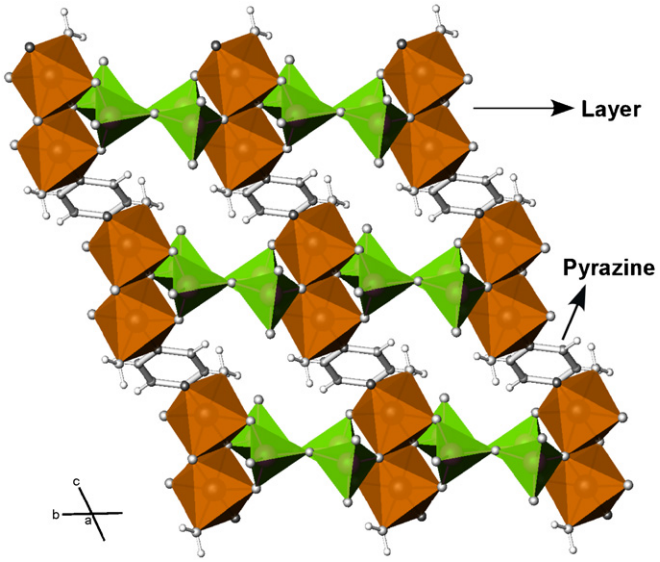

Fig. 3. Polyhedral view of the three-dimensional crystal structure of **1** showing the pyrazine molecules that link the layers.

between them by common edges to give rise to the layers in the (001) plane (see Fig. 2).

The pyrazine molecules link, through their nitrogen atoms, two Ni(II) cations belonging to different sheets give rise to a three-dimensional framework (Fig. 3), in which the hydrogen atoms from the water molecules point out towards the interlayer space.

In the $[Ni(1)O_5N]$ octahedral coordination polyhedra the Ni–O bond distances range from 2.055(3) to 2.107(3) Å, being the Ni–N bond lengths of 2.082(4) Å. The *cis*- and *trans*-angles in these octahedra range from 83.9(1) to 94.9(6)° and from 170.2(1) to 177.3(1)°, respectively. Distortion calculation was made for the Ni(1) coordination polyhedron comparing to the ideal geometries of polyhedra with coordination number 6 (octahedron and trigonal prism), using the model proposed by Muetterties and Guggenberger [13]. In this model real and ideal polyhedra are compared by evaluating their dihedral angles. The result confirmed the high regularity of $[Ni(1)O_5N]$ octahedron with a distortion of 3.9%. In the $[V(1)O_4]$ tetrahedron there are three kinds of bond distances. The longest bond with a mean value of 1.80(2) Å corresponds to the link between the V(1) atom with the O(2) and O(4)-oxygen atoms. The intermediate bond length, 1.709(3) Å, contain the oxygen atom, O(1). Finally, the short bond distance, 1.619(3) Å, corresponds to the link between the V(1) atom with the O(3)-terminal oxygen atom. In the $[V(2)O_4]$ tetrahedra, there are two V–O longer bonds [1.806(3) and 1.789(3) Å] and other two with a medium length [1.664(3) and 1.678(3) Å]. The mean bond lengths correspond to the bond oxygen atoms-O(5),O(6) linked to the Ni(II) cations, whereas the longer bond lengths contain the oxygen atoms-O(2),O(4) shared with the $[VO_4]$ adjacent tetrahedra.

3.2. Crystal structure of phase 2

The $Ni_3(C_4H_4N_2)_3(V_8O_{23})$ phase exhibits a complex three-dimensional structure constructed from $[NiO_4N_2]$ octahedra, $[VO_4]$ tetrahedra and the pyrazine molecules (see Fig. 4).

In this structure, the $[VO_4]$ tetrahedra are vertex shared, giving rise to twelve member rings, linked between them and extended along the [0−10] direction (Fig. 5). The $[NiO_4N_2]$ octahedra are linked to the pyrazine molecules forming $[Ni(C_4H_4N_2)O_4]_\infty$ infinite chains, disposed in the [100] direction (Fig. 6). The $[NiO_4N_2]$ octahedra are linked via vertices shared to the $[VO_4]$ tetrahedra, belonging to the rings, to give rise to the three-dimensional skeleton shown in Fig. 4.

In the $[Ni(1)O_4N_2]$ octahedra the bond distances range from 2.028(2) to 2.095(2) Å, being the greater bond distance that corresponding to the Ni1–N(2) bond [2.0952(2) Å]. The *cis*-angles are in the 88.71(9)–99.14(9)° range, being the *trans*-angles of 180.0(0)°. The $[Ni(2)O_4N_2]$ octahedra are more irregular. The bond lengths range from 2.034(2) to 2.106(2) Å, corresponding the longest bond distance, of 2.080(2) Å, to a Ni–N link. The *cis*- and *trans*-angles range from 86.00(9) to 92.23(8)° and 174.95(9) to 178.49(8)°, respectively. The distortion for the Ni(1) and Ni(2) coordination polyhedra was also obtained [13]. The results indicate the high regularity of $[Ni(1)O_4N_2]$ octahedra with a distortion of 3.1% and a slightly distorted octahedral geometry for the $[Ni(2)O_4N_2]$ octahedra with a distortion of 9.0%. In the four $[VO_4]$ tetrahedra the shortest distance for the V–O bonds is obtained for V(4)–O(9) with a value of 1.599(2) Å. The bonds between the metallic vanadium cation with oxygen atoms linked to the Ni(II) ions have a mean value of 1.655(5) Å. Finally, the V–O bond distances established with O(1)-oxygen atom, that is bonded simultaneously with other vanadium cation, are the longest, 1.831(2) and 1.773(2) Å.

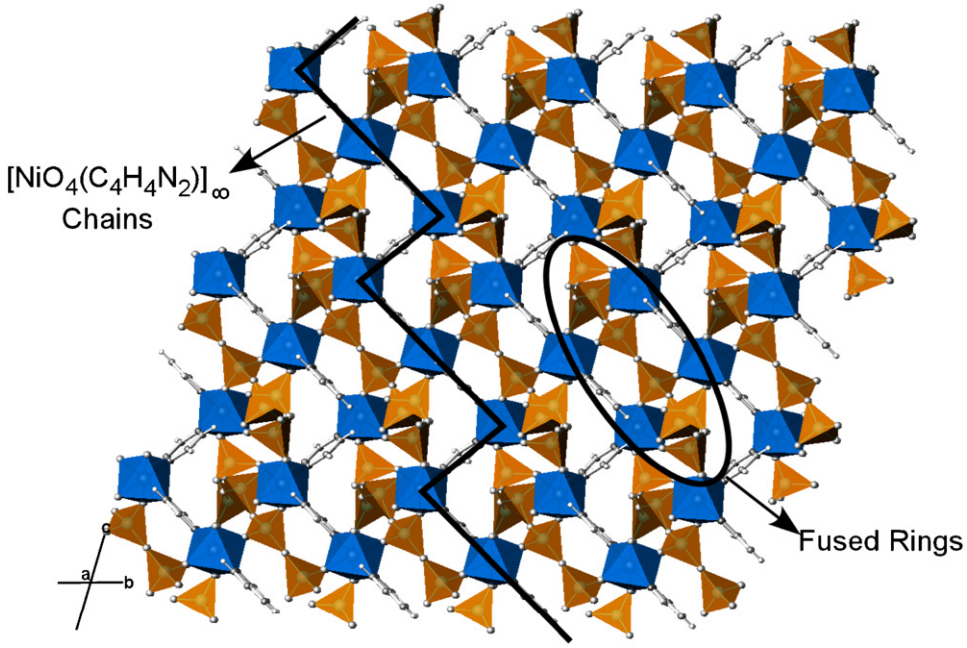

Fig. 4. Polyhedral view of the three-dimensional crystal structure of **2**.

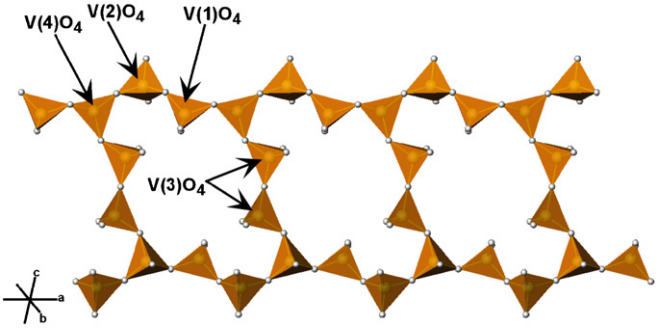

Fig. 5. Polyhedral view of the $[VO_4]$ tetrahedra forming the twelve member rings in **2**, along the *a*-axis.

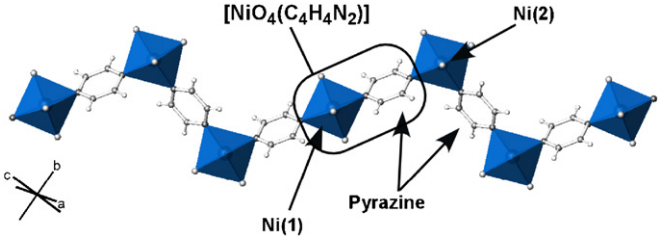

Fig. 6. Polyhedral view along the *a*-axis of the $[Ni(C_4H_4N_2)O_4]_\infty$ infinite chains, disposed in the [0−10] direction in compound **2**.

3.3. Diffuse reflectance spectroscopy

The diffuse reflectance spectrum of **1** shows the characteristic bands of the Ni(II) cation, d^8 ion, in a slightly distorted octahedral geometry. Two absorption bands ascribed to the spin-allowed transitions $^3A_{2g}\rightarrow{}^3T_{2g}$ and $^3T_{1g}(F)$ are observed at the following values 8820 and 14 700 cm^{-1}, respectively. The third spin-allowed transition $^3A_{2g}\rightarrow{}^3T_{1g}(P)$ is obscured by the charge transference bands, above 29 000 cm^{-1}. The spin-forbidden transition $^3A_{2g}\rightarrow{}^1E_g$ is detected as a shoulder on the second spin-allowed band at 12 580 cm^{-1}. The Dq and Racah parameters were calculated by fitting the experimental frequencies to an energy level diagram for octahedral d^8 systems [14]. The results obtained are Dq = 880, $B = 980$ and $C = 2700\,cm^{-1}$. The value obtained for the B parameter supposes a reduction of ca. 95% from that of the free Ni(II) ion (1030 cm^{-1}). These results are in the range usually found for octahedrally coordinated Ni(II) compounds [15].

3.4. Magnetic measurements

Magnetic measurements of **1** were performed on polycrystalline sample in the Zero Field Cooling (ZFC) and Field Cooling (FC) modes between 5.0 and 300 K at a magnetic field of 1000 Oe (Fig. 7). The thermal evolution of the ZFC and FC modes of the molar magnetic susceptibility, χ_m, shows reversibility in the entire range of temperatures studied. The χ_m vs. T curve increases with decreasing temperature and exhibits a maximum at 38 K indicating that magnetic ordering is reached, probably three-dimensional in nature taking into account the structural features of this phase. After 38 K, χ_m decreases up to 11 K and finally increases rapidly until 5.0 K. This last feature is probably due to the presence of Ni(II) paramagnetic centres, originated in the bulk of the sample by triturating. The non-irreversibility of the magnetic curves carried out at 1000 and 100 Oe, in the ZFC and FC modes, indicates the non-existence of weak

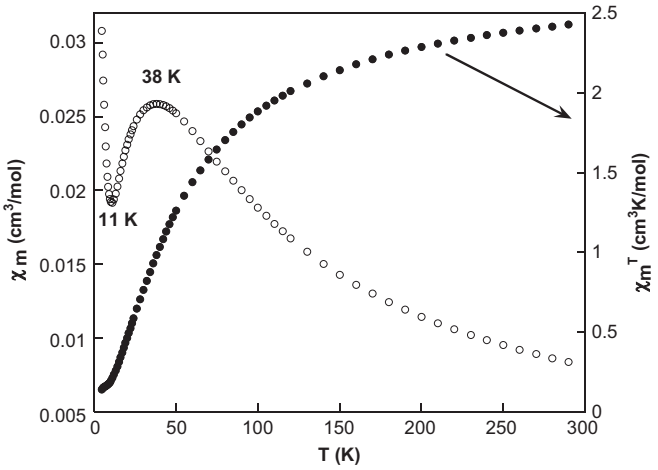

Fig. 7. Thermal evolution of the χ_m and $\chi_m T$ vs. T curves for **1**.

ferromagnetic interactions at low temperatures. The thermal evolution of $1/\chi_m$ follows a Curie–Weiss law at temperatures higher than 100 K, being the Curie and Curie–Weiss constants of $C_m = 2.858\,cm^3\,K/mol$ and $\theta = -50.4\,K$. The $\mu_{eff.} = 2.39\,\mu_B$ is characteristic of the Ni^{2+} cation [16]. The $\chi_m T$ vs. T product decreases continuously from 2.42 at 300 K to $0.14\,cm^3\,K/mol$ at 5.0 K. This result and the negative value of the Weiss temperature indicate that the main magnetic interactions are antiferromagnetic in nature.

Taking into account the crystal structure of **1**, four magnetic exchange pathways between the Ni(II) polyhedra can be distinguished. The values of the bond distances and angles for these magnetic pathways are shown in Table 2 with an asterisk. Three of them are intralayer pathways and the fourth one is an interlayer pathway (see Fig. 8). In Fig. 8, J_1 represents a superexchange pathway propagated through the O(1)-oxygen atoms belonging to the edge-shared between the Ni(II) dimers with an α angle of 95.95(1)°, which favor ferromagnetic interactions. In this pathway the magnetic $d_x2_{-y}2$ orbital of the Ni(II) cations and the p_x and p_y orbital belonging to the oxygens are involved. J_2 represents the super–superexchange pathway propagated through one $(VO_4)^{3-}$-vanadate anion in which the Ni–O(5)–V(2)–O(6)–Ni atoms are involved, being d_z2 the magnetic orbital. In the third exchange pathway, J_3 and J_4, indicate the super–superexchange pathway via two vanadate anions, being duplicated the sequence of atoms involved, Ni–O(5)/O(6)–V(2)–O(4)–V(1)–O(1)–Ni and Ni–O(5)/O(6)–V(2)–O(2)–V(1)–O(1)–Ni. In these two exchange pathways both the $d_x2_{-y}2$ and d_z2 metallic magnetic orbitals participate. Finally, the pathway J_5, represents the interlayer magnetic coupling established through the pyrazine molecules that link two Ni(II) cations belonging to different layers. The sequence of atoms involved in this pathway is Ni–N–C(1)–C(2)–N–Ni.

The mean value of these angles of 119.0(1)° is far away from the orthogonality, so ferromagnetic interactions are not observed [17]. This fact is in good agreement with the predominance of antiferromagnetic couplings between the Ni(II) cations, as was observed in the thermal evolution of the molar magnetic susceptibility.

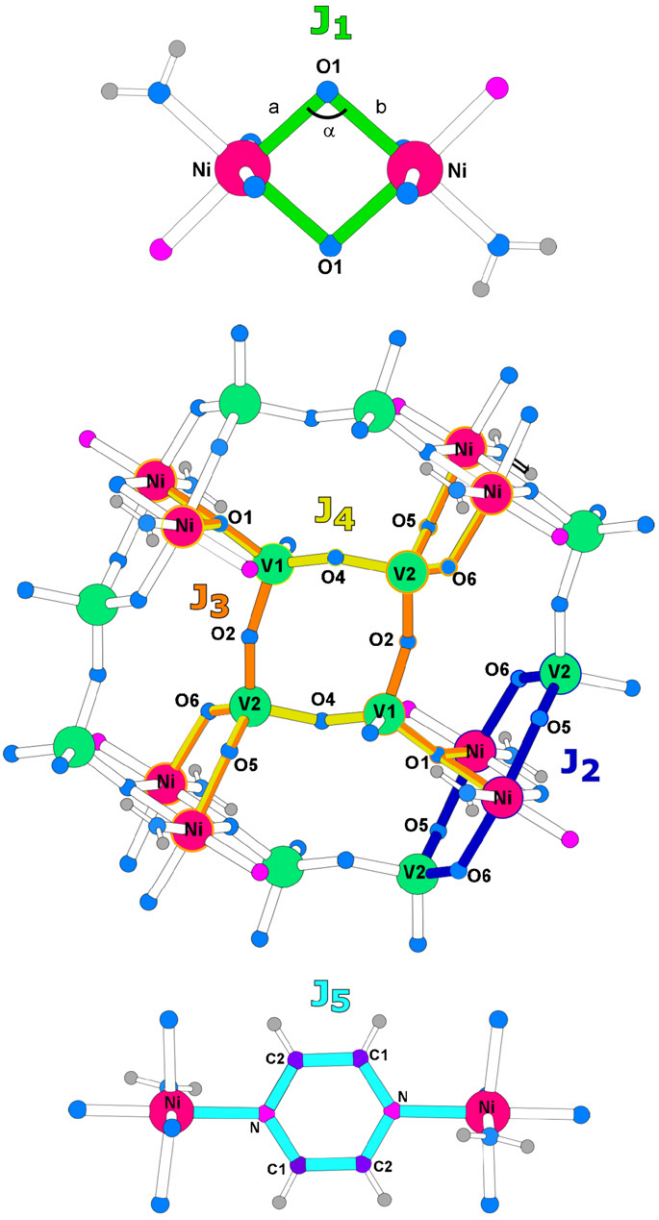

Fig. 8. Schematic representation of the possible magnetic exchange pathways for **1**.

4. Concluding remarks

Two new inorganic–organic hybrid materials based on the vanadium(V) oxide and Ni(II) coordination complexes have been synthesized under mild hydrothermal conditions. Both compounds, $Ni_2(C_4H_4N_2)(V_4O_{12})(H_2O)_2$ and $Ni_2(C_4H_4N_2)_3(V_8O_{23})$ exhibit three-dimensional crystal structures. The structure of the first one is formed by layers, constructed from edge-shared $[Ni_2O_6(H_2O)_2N_2]$ nickel(II) dimers octahedra and rings composed by four $[V_4O_{12}]$ vanadium(V) tetrahedra. These sheets are linked by

the pyrazine molecules, the thermal stability limit being of 280 °C. In the second one, the crystal structure is formed from edge shared $[VO_4]$ tetrahedra and $[NiO_4N_2]$ octahedra, that form $[NiO_4(C_4H_4N_2)]_\infty$ infinite chains, linked to the pyrazine molecules forming the 3D framework. Electronic spectroscopy measurements in solid state of the $Ni_2(C_4H_4N_2)(V_4O_{12})(H_2O)_2$ phase indicate the existence of Ni(II) cations with a slightly distorted octahedral geometry. Magnetic measurements on this phase show that the magnetic couplings are antiferromagnetic in nature.

Acknowledgments

This work has been financially supported by the "Ministerio de Educación y Ciencia" (MAT2004-02071), the "Universidad del País Vasco" (UPV/EHU) (9/UPV00130.310-16967/2004 and 9/UPV00169.310-13494/2001) and the "Fondo Europeo de Desarrollo Regional". We thank Dr. I. Orue ("Fondo Europeo Social" and "Ministerio de Ciencia y Tecnología") for magnetic measurements, respectively. Edurne S. Larrea thanks the UPV/EHU for funding.

Appendix A. Supplementary materials

References

[1] [a] T.G. Chirayil, E.A. Boylan, M. Mamak, P.Y. Zavalij, M.S. Whittingham, Chem. Commun. (1977) 33;
[b] P.Y. Zavalij, M.S. Whittingham, E.A. Boylan, V.K. Pecvharsky, R.A. Jacobson, Z. Kristallogr. (1996) 444;
[c] L.F. Nazar, B.E. Koene, J. Britten, Chem. Mater. 8 (1996) 327;
[d] Y. Zhang, R.C. Haushalter, A. Clearfield, Chem. Commun. (1996) 1055;
[e] Y. Zang, C.J. O'Connor, A. Clearfield, R.C. Haushalter, Chem. Mater. 8 (1996) 595;
[f] C.-Y. Duan, Y.-P. Tian, Z.-L. Lu, X.-Z. You, X.-Y. Huang, Inorg. Chem. 34 (1995) 1;
[g] G. Huan, J.W. Johnson, A.J. Jacobson, J.S. Merola, J. Solid State Chem. 91 (1991) 385.
[2] S. Aschwanden, H.W. Schmalle, A. Reller, H.R. Oswald, Mater. Res. Bull. 28 (1993) 45.
[3] J.R.D. DeBord, Y. Zhang, R.C. Haushalter, J. Zubieta, C.J. O'Connor, J. Solid State Chem. 122 (1996) 251.
[4] Y. Zhang, J.R.D. DeBord, C.J. O'Connor, R.C. Haushalter, A. Clearfield, J. Zubieta, Angew. Chem. Int. Ed. Engl. 35 (1996) 989.
[5] K. Nakamoto, Infrared and Raman Spectra of Inorganic and Coordination Compounds, Wiley, New York, 1997.
[6] Powder Diffraction File-Inorganic and Organic, ICDD, files nos. (a) 76-0359, (b) 38-0285.
[7] A.C.T. North, D.C. Philips, F.S. Mathews, Acta Crystallogr. A 24 (1968) 351.
[8] Oxford Diffraction Ltd. CRYSALIS 1.171.29 version, 2006.
[9] G.M. Sheldrick, SHELXS 97: Program for the Solution of Crystal Structures, University of Göttingen, Germany, 1997.
[10] G.M. Sheldrick, SHELXL 97: Program for the Rietveld Refinement of Crystal Structures, University of Göttingen, Germany, 1997.
[11] L.J. Farrugia, J. Appl. Crystallogr. 32 (1999) 837.
[12] T. Hahn (Ed.), International Tables for X-ray Crystallography, vol. IV, Kynoch Press, Birmingham, England, 1974 p. 99.
[13] E.L. Muetterties, L.J. Guggenberger, J. Am. Chem. Soc. 96 (1974) 1748.
[14] A.B.P. Lever, Inorganic Electronic Spectroscopy, Elsevier Science Publishers B.V., Amsterdam, Netherlands, 1984.
[15] [a] J.M. Rojo, J.L. Mesa, J.L. Pizarro, L. Lezama, M.I. Arriortua, T. Rojo, Mater. Res. Bull. 31 (8) (1996) 925;
[b] J.M. Rojo, J.L. Mesa, J.L. Pizarro, L. Lezama, M.I. Arriortua, T. Rojo, J. Solid State Chem. 132 (1997) 107;
[c] J.L. Mesa, J.L. Pizarro, L. Lezama, J. Escobal, M.I. Arriortua, T. Rojo, J. Solid State Chem. 141 (1998) 508.
[16] R.L. Carlin, Magnetochemistry, Springer, Berlin, Heidelberg, 1986.
[17] J.B. Goodenough, Magnetism and Chemical Bond, Interscience, New York, 1963.